The contribution of different aerosol types to direct radiative forcing over distinct environments of Pakistan inferred from the AERONET data

The contribution of different aerosol types to direct radiative forcing over distinct environments of Pakistan inferred from the AERONET data

Rehana Khan[a,c], Kanike Raghavendra Kumar[b,a*], Tianliang Zhao[a,**], Gohar Ali[a,d]

[a]*Collaborative Innovation Centre on Forecast and Evaluation of Meteorological Disasters, Key Laboratory of Meteorological Disaster, Ministry of Education (KLME), International Joint Laboratory on Climate and Environment Change (ILCEC), Key Laboratory for Aerosol-Cloud-Precipitation of China Meteorological Administration, School of Atmospheric Physics, Nanjing University of Information Science and Technology, Nanjing 210044, Jiangsu, China.*

[b]*Department of Physics, Koneru Lakshmaiah Education Foundation (KLEF), Vaddeswaram 522502, Guntur, Andhra Pradesh, India.*

[c]*Department of Physics, Higher Education, Government of Khyber Pakhtunkhwa Peshawar 25000, Pakistan.*

[d]*Pakistan Meteorological Department, P.O. Box 44000, Sector H-8/2, Islamabad 45710, Pakistan.*

***Corresponding authors**

Email: rkkanike@kluniversity.in (K. R. Kumar); tlzhao@nuist.edu.cn (T. L. Zhao)

Abstract

To quantitatively estimate and analyze the contribution of different aerosol types to radiative forcing, we thoroughly investigated their optical and radiative properties using the Aerosol Robotic Network (AERONET) data (2007-2018) over an urban-industrial (Lahore) and coastal (Karachi) cities located in Pakistan. The contribution of inferred aerosol types following the threshold applied for FMF_{500} versus SSA_{440} and $EANG_{440-870}$ versus $AANG_{440-870}$ were found the highest for pure dust (PUD, 31.90%) followed by polluted continental (POC, 24.77%) types of aerosols, with moderate contribution was recorded for polluted dust (POD, 20.92%), organic carbon dominating (OCD, 11.85%), black carbon dominating (BCD, 8.77%) and the lowest for the non-absorbing (NOA, 1.79%) aerosol type. Seasonally, the mean (±SD) aerosol optical thickness at 440 nm (AOT_{440}) was found maximum (0.73±0.36) for PUD type in summer and minimum for BCD (0.25±0.04) during spring at Karachi. However, the mean (±SD) AOT_{440} varied from 0.85±0.25 during summer to 0.57±0.30 in winter at Lahore, with the highest contributions for POC (29.91%) and BCD (22.58%) and the lowest for NOA (5.85%) type of aerosols. Further, the intensive optical properties showed significant temporal and spectral changes and the complexity of inferred aerosol types over the study sites. The results are well substantiated with the air mass analysis obtained from the concentration weighted trajectory (CWT) model for different aerosol types. The Santa Barbara DISORT Atmospheric Radiative Transfer (SBDART) model revealed the strong presence of BCD aerosol type led to a surface (BOA) and top of atmosphere (TOA) forcing of -70.12, -99.78 Wm^{-2} and -9.60, -19.74 Wm^{-2}, with an annual heating rate of 2.10 and 2.54 $Kday^{-1}$, respectively, at Karachi and Lahore sites.

Keywords: Aerosol types; Aerosol optical thickness; Fine mode fraction; Single scattering albedo; Absorption Ångström exponent; Radiative forcing.

1. Introduction

Rapid urbanization and industrialization have led to an increase in air pollution over several cities in Asia during recent years. The South Asian region is one of the most densely populated and distinct geographical domains with multiple emission sources, where the aerosols have not only affect the regional and local climate, apart from the hydrological scale but, indirectly alter the Earth's radiation budget (IPCC. 2018). However, two megacities in Pakistan of the Asian continent, the coastal location of Karachi and landlocked urban-industrial environment of Lahore, play a dominant role in the distribution of air pollutants. Since a long time, the global monitoring of aerosols through the ground-based measurements from several networks (e.g., the AErosol RObotic NETwork (AERONET)) provides a unique chance to characterize them by varying types (Choi et al., 2016), and assess their impacts on radiative forcing (Tiwari et al., 2015; Kumar et al., 2020).

In the recent decades, numerous authors (e.g., Srivastava et al., 2012; Kaskaoutis et al., 2012; Alam et al., 2012, 2014; Bibi et al., 2016; Kumar et al., 2013, 2017, 2018, 2020; Boiyo et al., 2019; Khan et al., 2019) had benefitted from the AERONET retrieved direct and inversion products for the characterization of aerosol optical (e.g., aerosol optical thickness (AOT); Ångström exponent (ANG), single scattering albedo (SSA)) and microphysical (volume size distribution (VSD), effective radius (R_{eff})) properties over different places in the world. In this study, a classification technique utilized from the works of Lee et al. (2010) was deployed to characterize different absorbing and non-absorbing aerosol types using the aerosol optical parameters (such as the fine-mode fraction of AOT measured at 500 nm (FMF_{550}) and SSA_{440}. A brief explanation of aerosol optical properties and their discrimination of aerosol types can affect aerosols on the simulation of radiative forcing. Recent studies (Choi et al., 2016; Kumar et al., 2018; Boiyo et al., 2019; Rupakheti et al., 2019; Shin et al., 2019; Kumar et al., 2020) have shown a statistically significant and robust association between the aerosol optical properties and radiative forcing inferred from various aerosols. A few studies (Che et al., 2018; Choi et al., 2016) have discussed the effect of different aerosol types on radiative forcing and heating rate, with the long-term ground-based data. A recent study by Khan et al. (2019) had identified key aerosol types from six AERONET sites over Southeast Asia, where they found dominant contributions of biomass burning and urban-industrial aerosol-types followed by the mixed nature of aerosols. An earlier report by Bibi et al. (2017) used the AERONET data to characterize the aerosol optical properties by implementing multiple clustering techniques for the seasonal classification of aerosol-types during 2007-2013 over the Indo-Gangetic Plain (IGP), which include Lahore and Karachi apart from the other sites. Along these lines, Shaheen et al. (2019) adopted a clustering technique by using the long-term (2005-2017) AERONET retrieved parameters over Beijing, China.

The current work has been unique of its kind in re-iterating the thresholds to discriminate the aerosol types following the clustering techniques given in the previous works (Table S1 of Supplementary Material (SM)). This study has been conducted following the long-term measured ground-based AERONET data (2007-2018) to understand the contribution of major absorbing aerosol types, and their associated impact on radiative forcing in a 3D-way over two megacities (Karachi and Lahore) prevailed with distinct environments in Pakistan. The dominant aerosol types and their contribution to the atmospheric column abundance of aerosols are performed in terms of the temporal and spectral variations of AOT, SSA, ANG, and VSD following the clustering framed of FMF versus SSA. We compared our results observed to those from previous studies for the same sites to ensure the validity of the present approach. Further, we identified the potential source contribution of inferred aerosol types at both the locations using the concentration-weighted trajectory (CWT) method following the meteorological data provided by the Hybrid Single-Particle Lagrangian Integrated Trajectory (HYSPLIT) model. The ARF and associated heating/cooling rates in the atmosphere and its efficiency inferred for the aerosol types have been quantified on temporal scales using the Santa Barbara DISORT Atmospheric Radiative Transfer (SBDART) model over the two sites.

2. Data and methods

2.1. Site description

The ground-based aerosol climatology is derived over the two AERONET sites located in Pakistan to account for the heterogeneity in aerosol optical, microphysical, and radiative properties inferred from various aerosol types in the most recent years (2007–2018). The selected regions of interest comprise two important high aerosol laden sites: Karachi (24.87°N, 67.03°E, 26 amsl) and Lahore (31.54°N, 74.32°E, 712 amsl) where they were identified on the spatial map (with red color solid circles) representing the topography of the country (Fig. 1). Being proximity to an immense the Thar Desert (Lahore) and the Arabian Sea (Karachi), both the study sites experience the influence of dust and marine aerosols mostly during the spring and summer seasons (Alam et al., 2012, 2014; Bibi et al., 2016; Khan et al., 2019). The pollutants at these two stations are, thus, a complex mixture of natural and anthropogenic (densely populated and urban-industrialized) aerosols that cause variability in the characterization of aerosol optical properties and radiative effects (Bibi et al., 2017).

The monthly mean variations of major meteorological parameters (such as air temperature (AT), wind speed (WS), relative humidity (RH), and rainfall (RF)) obtained from the Pakistan Metrological Department (PMD) measured during 2007-2018 over the two sites is shown in Figs.

1a-b. The results revealed that both the places are generally influenced by enhanced precipitation during the humid and hot summers, characterized by relatively high temperatures and RH. The WS remains moderately varied in the range 0.71–3.9 ms^{-1} and 0.3–1.22 ms^{-1} over Karachi (Fig. 1a) and Lahore (Fig. 1b), respectively. However, the minimum (maximum) ATs occurred in January (June) with 19.65 °C (32.04°C) and 12.95 °C (33.21°C) for Karachi and Lahore, respectively. Besides, due to its proximity to the Arabian Sea, the RH at Karachi remains consistently high (~81%, Fig. 1a), with a significant influence on the number of aerosol processes (Alam et al., 2012). For the annual assessment, we considered four different seasons mentioned as follows: spring (from March to May), summer (June to August), autumn (September to November), and winter (December to February).

2.2. Instrument and data

The primary data set used constituted the remotely-sensed ground-based measurements conducted by the AERONET's CE-318 Sun photometer (Cimel Electronique, France), and the retrieved data for all the stations given by the AERONET is wide open and downloaded at https://aeronet.gsfc.nasa.gov/. In the present work, we used the Version 3.0 and Level 1.5 (cloud screened) spectral AOT data in the wavelength range of 440–1020 nm, and ANG estimated for the wavelengths between 440 and 870nm. Moreover, the other inversion products include absorption AOT and ANG (AAOT, AANG), asymmetry parameter (ASP), extinction AOT and ANG (EAOT, EANG) used in work are obtained in the spectral range of 440-1020 nm, and VSD. The uncertainty in AOT under cloud-free conditions is ±0.01 and ±0.02 for higher and lower wavelengths, respectively (Eck et al., 1999). Whereas, the uncertainty involved in the retrieved inversion products of SSA_{440} and ASP_{440} (with AOT_{440}> 0.40) were found ±0.03 and ±0.02, respectively (Dubovik et al., 2006). While analyzing, we noticed gaps in the data are due to thick cloud cover, more precipitation days, calibration procedure, and system malfunction. It is mentioned that the recent collaboration (AERONET) provides AOT data, in three different quality levels: Level 1.0 (unscreened), Level 1.5 (cloud-screened and quality controlled), and Level 2.0 (quality-assured) (Holben et al., 1998). The reason behind using level 1.5 instead of level 2.0 data is that level 2.0 datasets are not provided by the AERONET since late 2017, at the observation locations. Also, the recently released version 3.0 data products are capable in advanced cloud screening, and automated data quality assurance with higher air masses up to 7 (in level 1.5) in contrast with version 2.0 (which is up to 5) (Khan et al., 2019; Kokkalis et al., 2018; Kumar et al., 2020). Hence, owing to the excellent availability of data count provided with the real-time and continuous long-term duration of data, level 1.5 was utilized for analyzing the aerosol characteristics in its different types in this study (Fig. S1 of SM).

2.3. Cluster technique for aerosol typing

A study in the classification of absorbing and non-absorbing aerosol types over different locations was carried out based on the approach proposed by Lee et al. (2010) via., the SSA_{440} versus FMF_{500} relationship previously conducted by several authors (Table S1 of SM) (e.g., Srivastava et al., 2012; Tiwari et al., 2015; Choi et al., 2016; Chen et al., 2016; Kang et al., 2016; Moreno et al., 2019). Lee et al. (2010) characterized aerosol types based on dominant size mode (FMF_{500}) and radiation absorptivity (SSA_{440}), over North Africa and the Arabian Peninsula by adopting a safety margin of 0.2, by FMF to be higher than 0.6 (less than 0.4) as are defined fine-mode (coarse-mode) aerosols. Aerosols in the safety margin of the thresholds (that is, between 0.4 and 0.6) are classified as a 'mixture' of coarse- and fine-mode aerosols (Fig. S2 and Table S1of SM).

The main types of aerosols observed from the clustering of SSA_{440} versus FMF_{500} were divided into six categories, namely, Pure Dust (PUD; only dust dominating aerosols), Polluted Dust (POD; dust dominating relative to anthropogenic aerosols), polluted continental (POC; anthropogenic dominating relative to dust aerosols), highly absorbing (BCD; only anthropogenic dominating due to black carbon aerosols), low absorbing (OCD; only anthropogenic dominating due to organic carbon aerosols), and non-absorbing (NOA; aerosols with no absorption, i.e., scattering nature). Values of $FMF<0.4$ and $SSA>0.9$ corresponds to PUD type, and $FMF<0.4$ with $SSA\leq0.9$ represents POD type; whereas, the thresholds with $0.4 \leq FMF \leq 0.6$ and $0.4 \leq SSA \leq 0.9$ is associated with POC type of aerosols. However, for all the values of $FMF>0.6$ with $SSA<0.9$, $0.9 \leq SSA \leq 0.95$, and $SSA > 0.95$ indicates BCD, OCD, and NOA types of aerosols, respectively. Besides, the other aerosol optical parameters such as $AANG_{440\text{-}870}$ and $EANG_{440\text{-}870}$ are also clustered together to investigate the dominant aerosols representing their annual and seasonal variations over the sites; however, both the methods are found to be well associated with each other presenting the similar dominant type of aerosols. To supplement this method, the threshold applied on $AANG_{440\text{-}870}$ ($EANG_{440\text{-}870}$) for BB (biomass burning type of aerosols which are comparable with BCD type), Dust (corresponds to PUD+POD), and UI (urban-industrial aerosol type similar to NOA) follow 1.1-2.3 (0.8-1.7), 1.0-3.0 (0-0.4) and 0.6-1.2 (0.8-1.6) respectively, by utilizing the approach adopted from Giles et al. (2012) and Rupakheti et al. (2019).

2.4. Source receptor model

The CWT method is the most widely used technique to identify the distant emission sources of air masses for the different aerosol types (Hsu et al., 2003). Here, we used the same model provided the AOT_{440} input data related to the following four aerosol types (Dust (PUD+POD), POC, BCD, NOA) about the height of 500 m above ground level and for the time duration of -72h (i.e., three days backward) to capture the potential source areas affecting the receptor sites (Karachi and Lahore). This approach is based on the TrajStat plug-in used in the GIS-receptor based model software and is found elsewhere (Wang et al., 2009; http://www.meteothinker.com/Documents/Wang_TrajStat_Manuscript.pdf). Additionally, each CWT value reflects a conditional probability describing the potential contribution of a grid cell of the high pollutant loadings at the receptor site; however, this approach is capable of distinguishing primary sources from moderate ones (Hsu et al., 2003). In the CWT method, each grid cell is assigned a weighted concentration by averaging the sample concentrations, which have associated trajectories that crossed the grid cell as follows:

$$C_{ij} = \frac{\sum_{h=1}^{M} C_h \times \tau_{ijh}}{\sum_{h=1}^{M} \tau_{ijh}} \times W(n_{ij}) \qquad (1)$$

where C_{ij} is the mean weight concentration of the back trajectory 'h' in the ij cell; C_h represents inferred aerosol type concentration (here AOT) in the trajectory 'h' through ij cell; τ_{ijh} represents the time that trajectory 'h' resides in the ij cell. W (n_{ij}) used in the CWT is to reduce the uncertainty in cells.

2.5. Radiative Transfer model

The daily net fluxes obtained for the inferred aerosol types at the BOA and TOA of the atmospheres were calculated for the clear-sky shortwave (0.3–4.0 μm) direct ARF using the sun/sky radiometer measured spectral values of AOT, ANG, SSA, and ASP as inputs into the SBDART model (Ricchiazzi et al., 1998). Besides these optical parameters, the surface albedo, which plays a vital role in the forcing calculation was obtained over the study sites from the Aura Ozone Monitoring Instrument (OMI-3) reflectivity data set as well as retrieved from the

AERONET inversion products. Besides, the diurnally averaged radiative forcing at the TOA and BOA was obtained from the AERONET at every one-hour interval for a 24 h period, with an accuracy of ±2 Wm^{-2} (Kumar et al., 2017). Moreover, the model is capable of estimating the radiative flux within 2% of direct and diffuse irradiance measurements (Kang et al., 2016), and has been widely used to solve the radiative transfer problems in several studies around the world (e.g., Alam et al., 2012; Yu et al., 2016; Boiyo et al., 2019; Kumar et al., 2020).

4. Results and discussion

4.1. Classification of aerosol types

Fig. 2 presents the scatter plots between SSA_{440} and FMF_{500} as a function of AOT_{440} observed at Karachi and Lahore to infer different aerosol types. A wide range of SSA (0.86-0.92) was found at both the sites for every kind of aerosol. However, the deviation in FMF at Lahore was evident only for BCD, OCD, and NOA types of aerosols, attributed to changes in emission sources. It is evident from the earlier studies that the pollutants from the burning of agricultural residue, especially in the harvesting season (autumn), contribute significantly to organic (OCD) aerosols. Besides, secondary aerosols from high traffic flow (fossil fuel burning) and a large amount of coal consumption for household heating and domestic cooking at these locations is the second reason for the observed variations in these types of aerosols. Figs. 2c-d shows the monthly fluctuations in the occurrences of dominant aerosol types. Statistically, the occurrence represents the number of times dominant aerosol types occur during the valid operating hours of the instrument in the almucantar geometry, being found the highest for POD and BCD aerosol types during April and December at Karachi and Lahore, respectively. Further, the statistics illustrate that there was the more frequent occurrence found for PUD types over Karachi between April and June, which is mainly due to a large amount of windblown desert and mineral dust particles, considering that the site (Karachi) is located on the coast of Arabian Sea. The OCD (BCD) type is also found high in November and December months over Karachi (Lahore). However, the occurrence range is low for NOA comparatively, throughout the period, especially at Karachi, attributed to the difference in population, geography, elevation (Fig. 1), and use of anthropogenic sources at the study sites. Another reason behind may be the availability of fewer data points attributed to some specific flaws, including cloud covers, technical errors, and instrument sent for calibration, etc. The occurrence of a more substantial contribution by POC and BCD types at Lahore and PUD over Karachi is related to anthropogenic particles (Tiwari et al., 2015), and sea salt aerosols from the marine environment (Bibi et al., 2016). The carbonaceous (absorbing) aerosol types such as BCD and OCD revealed a sharp winter peak over both the sites. In particular, the contribution of BCD type increased from October to December, while the OCD type increased during October-February. The PUD (31.90%) followed by POC (24.77%) types of aerosols were recorded among the highest contribution relative to the rest of the aerosol types, being dominant during the spring and autumn seasons, respectively (Fig. 2e). Whereas, the NOA (1.79%) followed by the BCD (8.77%) aerosol types were found minimum in all seasons, with the lowest in spring at Karachi (Fig. 2e). However, the OCD (11.85%) type of aerosols contributed moderately to the aerosol load at both the sites.

The season-wise distribution of scatter plots between $AANG_{440-870}$ and $EANG_{440-870}$ to classify different aerosol types is presented in Fig. 3. Three prominent classes of aerosols were reported over the sites such as dust, BB, and UI. Absorption and extinction thresholds revealed coarse-mode dominating particles at both the sites especially, during the spring and summer seasons, while fine-mode anthropogenic aerosols were found dominating during winter and autumn. However, both the clustering techniques (FMF versus SSA and AANG versus EANG) showed similar results and revealed prominent consistency between them. The results obtained in this study are identical to that of Bibi et al. (2016) and Alam et al. (2016) utilizing clustering analysis between AANG and EANG to classify various types of aerosol over the two sites.

4.2. Variations in aerosol optical properties

The annual contribution representing different seasons of varied aerosol types for AOT_{440} observed at Karachi and Lahore is shown in Figs. 4a-b. The maximum occurrences were found for NOA type of aerosols in all seasons, with a maximum AOT_{NOA} ranging from 0.87±0.51 (Lahore) to 0.72±0.13 (Karachi) in summer attributed to hygroscopic growth of aerosols. Whereas, both the sites have observed the highest AOT for OCD during spring and autumn seasons, with the mean (±SD), ranged between 1.27±0.63 (Lahore) and 0.63±0.26 (Karachi) (Table 1), strongly related to the seasonal pollution (e.g., dust, haze, and smog) events observed frequently over the IGP region from past few years (Alam et al., 2018). Bibi et al. (2016) and Tiwari et al. (2015) have shown a similar distribution of absorbing aerosols for the same sites, which peaks during the autumn attributed to long-range transport and locally generated pollutants. Besides, the dominant components at the coastal site are sea salt and inorganic aerosol particles, which are an active agent for highly scattering particles. The seasonal mean $ANG_{440-870}$ depicted with the maximum (1.30) and minimum (0.40) during winter and autumn for NOA and PUD, respectively. It further tends to decrease gradually up to 0.15 in spring, as observed at both the sites (Figs. 4c-d, Table 1). The low value of mean (±SD) ANG (0.33±0.13) with relatively high AOT (0.59±0.28) at Karachi attributed to the enhanced dust and sea-salt aerosols transported from the Middle East, Arabian Sea, and the Thar and Cholistan Deserts of Pakistan. Moreover, the comparatively high AOT (0.63±0.33) and ANG (1.21±0.13) at Lahore is due to the occurrence of more BCD type of aerosols suggests the dominant presence of fine-mode

287 aerosols mainly from biomass burning and industrial-vehicular emissions transported from the most prominent economic zone of IGP.

289 Figs. 4g-h shows the seasonal variations of SSA_{440} with more scattering (> 0.93) found during the summer for NOA, and POC aerosol types, are likely due to the influence of dust particles transported from the desert regions. However, the lower (strong absorption) (<0.81) in winter for BCD type could be due to the effect of biomass burning activities at both the sites. Another reason is, both places are under the influence of heavy air pollution due to haze and smog caused by the high aerosol loading due to more anthropogenic activities and dense population. Moreover, the seasonality in aerosol properties over the regions is also due to local emissions, apart from the change in the meteorological phenomenon (Khan et al., 2019).

297 The 3D scatter plot (Fig. 5) shows that sliding at the shorter scale range, of EANG and SSA, resulted in Dust (PUD+POD) type aerosols at both the stations with slightly high data points for Karachi site mainly associated with natural desert surfaces and locally produced dust and marine particles with high winds. However, going towards a higher scale range of SSA and EANG combined with the maximum EAOT results BCD (POC) in predominance for Karachi (Lahore) followed by OCD and NOA aerosol type, being consistent with the prevalence of regional anthropogenic activities and biomass burning mainly in the spring season.

304 Furthermore, the CWT model analysis revealed that the air masses traveled predominantly from the marine environments (the Arabian Sea) located in the south, and arid regions in the east (from the Thar Desert in India) and west (Afghanistan) that regulate the columnar aerosol loading at both the sites (Fig. 6). Owing to the annual dust episodes, the CWT revealed significant influence (CWT_{Dust} > 0.9) of potential sources from the dust areas over the coastal site (Karachi) (Fig. 6), followed by CWT_{POC} (~0.8) and CWT_{BCD} (<0.7) over Lahore, moderately

affected due to CWT_{POC} (<0.6), and low CWT_{Dust} (<0.4) over Karachi and Lahore sites, respectively, indicates significant diverse contributions from the regional aerosol sources to AOT_{440} primarily, governed by the distant and localized sources.

4.3. Particle volume size distribution

Fig. 7 gives the seasonal mean changes observed in aerosol VSD patterns for inferred aerosol types, whereas the annual mean changes shown in Fig. S5a-b and S6a-h of SM are noted at 22 size bins with different radii between 0.05 and 15.0 μm during the entire study period. The gray shaded area indicates the standard deviation of the mean for a given aerosol-type. The VSDs exhibited almost bimodal structure in all seasons, with the secondary peak (coarse-mode) relatively higher than the primary (fine-mode), indicating the varied contribution of particles. There are several possible explanations for the observed differences between the two modes; however, the variation of VSD significantly influences the radiative properties of aerosols. The VSD curves for the PUD and POD aerosol-types were more easily distinguishable than the rest of all types. The volume particle concentration of coarse-mode was found higher in all seasons for most of the aerosol-types, except NOA. The fine-mode peak was prominent throughout the study period at both the study sites attributed to the inferred aerosol-type, environment, and meteorological conditions (Alam et al., 2012). As expected, the PUD type was found relatively higher over Lahore during spring (0.80±0.03) and summer (0.35±0.02) seasons than at Karachi, which is (0.28±0.01) and (0.24±0.04), respectively. This is evident and consistent with the previous studies (e.g., Bibi et al., 2016) that the geographical location of Lahore city with its higher proximity to the dust source regions (e.g., Thal, Thar, and Cholistan Deserts) compared to Karachi, apart from the long-distant transport of dust particles from the deserts of Arabian Peninsula. The annual mean (±SD) particle volume concentration (and R_{eff}) in the fine-mode was noticed high for $PUD_{Karachi}$ which is 0.37±0.01 $\mu m^3 \mu m^{-2}$ (0.12±0.01 μm) followed by NOA_{Lahore} and OCD_{Lahore} with 0.15±0.07 $\mu m^3 \mu m^{-2}$ (0.20±0.04 μm) and 0.12±0.07 $\mu m^3 \mu m^{-2}$ (0.18±0.03 μm), respectively. The low was observed for $POD_{Karachi}$ with 0.02±0.01 $\mu m^3 \mu m^{-2}$ (0.11±0.01 μm) (Table 3). Moreover, a noticeable increase in coarse-mode volume concentration was observed for the OCD types during the winter and autumn season at both the sites, attributed to the seasonal inputs of plant residue, soil and desert dust, and biomass burning components.

4.4. Implications to radiative forcing

The monthly (Fig. S7 and S8 of SM) and seasonal (Fig. 8) mean changes of radiative forcing was estimated for different aerosol types at the TOA and BOA using the SBDART model for the two sites during the entire study period. The radiative forcing at the BOA revealed a strong influence during the study period. However, the variability in TOA forcing is weaker, presenting maximum values for PUD in June (−93 W m^{-2}) and July (−86 W m^{-2}) and minimum in October (−31 W m^{-2}) for OCD at Karachi (Fig. S7 of SM). It is observed that amongst all the types, the BCD aerosol-type has registered the highest positive ATM forcing in January (65 W m^{-2}) and February (63 W m^{-2}), with an annual mean of 56±6.8 Wm^{-2} and corresponding heating rate of 2.31 $Kday^{-1}$ (Fig. 8). Additionally, the forcing obtained at both the sites was highly dependent on the aerosol column load, which increases with the AOT and its type, especially for black carbon and organic carbon types during the winter and spring seasons. Likewise, the decreasing tendency in RF seen manifest, affiliated with the reduced AOT values for POD and PUD aerosol types, during winter and summer, respectively (Fig. 8 and S7, S8 of SM), which ultimately affect the range of HR in the upper atmosphere over the study regions (Garcia et al., 2008).

It is observed that the atmospheric HR of fine-mode aerosol increases with the AOT at both the sites, with the mean values larger than ~2.1 $Kday^{-1}$. The highest HR associated with the presence of BCD aerosol-type was found in Karachi varied between 1.95 $Kday^{-1}$ and 2.31 $Kday^{-1}$ during winter and autumn seasons, respectively, with the corresponding $AOT_{440,}$ found to be > 0.5 (Figs. 8a-d). The seasonality in TOA forcing is due to BCD type of aerosols significantly associated with various assumptions such as low precipitation rate in winter, dry and cold weather conditions resulted in increased household burning, biomass/agriculture residue burning (Bibi et al., 2017) and so on. However, the more amount of rainfall during June and July affects the growth of vegetation, indirectly changes the surface cover, and hence, the surface albedo in summer (Kang et al., 2016; Boiyo et al., 2019), is another crucial reason for the fluctuation in ARF. As such, it can be inferred that aerosol and other atmospheric constituents, in addition to clouds, play a significant role in the attenuation of solar radiation over the sites.

In contrast, Lahore showed the highest BOA (−158.21 W m^{-2}) and ATM forcing (+99.7 W m^{-2}) for PUD and BCD aerosol types, respectively, during the spring, with HR of 2.31 $Kday^{-1}$ (Figs. 8f-i). However, the lowest radiative forcing was observed for NOA with the BOA and ATM forcing values of −80.03 and +60.7 W m^{-2}, respectively, along with the HR of 1.4 $Kday^{-1}$, which is slightly more than the value (~1.02 $Kday^{-1}$) reported by Kumar et al. (2018) over Kanpur in IGP, and Bibi et al. (2017) and Alam et al. (2014) for the same study sites of Pakistan. Numerous studies have emphasized the significant role of radiative forcing by absorbing aerosols over the same regions (Alam et al., 2014; Tiwari et al., 2015; Bibi et al., 2017; Khan et al., 2019). Nevertheless, it is seen that the BOA forcing for PUD/POD aerosol-type becomes a minimum than that of the TOA forcing due to less scattering by different aerosol types at both the sites. Apart from this, the radiative forcing is highly dependent on SSA (Srivastava et al., 2012; Boiyo et al., 2019; Kumar et al., 2020). For lower SSA, the ARF found highly negative.

Further, the ARFEs (the rate of forcing per unit AOT) (Fig. 8 and Figs. S9, S10 of SM) showed a strong influence during winter/autumn with maximum values for BCD_{BOA} in January (−230 W m^{-2} τ^{-1}) and February (−239 W m^{-2} τ^{-1}), and minimum for NOA_{BOA} during autumn in October (−105 W m^{-2} τ^{-1}) and September (−100W m^{-2} τ^{-1}) at Karachi and Lahore, respectively. A distinct seasonal variability can be found for ARFEs at TOA. It is observed that amongst all the types, the PUD aerosol-type has registered the highest TOA efficiency in December (-80 W m^{-2} τ^{-1}) at Karachi followed by Lahore (-78 W m^{-2} τ^{-1}) and lowest for BCD type during August (-20 W m^{-2} τ^{-1}) and January (-30 W m^{-2} τ^{-1}) for Lahore and Karachi, respectively suggested, more absorbing aerosols produce a lower forcing efficiency at the TOA.

5. Summary of conclusions

In the present work, we investigated and compared the characteristics of aerosol types over Karachi and Lahore via the cluster analysis of optical, microphysical, and radiative properties obtained from 12 years of ground-based AERONET data set. The primary purpose of the present work is to investigate and understand the heterogeneity in different aerosol species, its origin, and the associated direct radiative impacts on regional climate and their heating effect. The implementation of two different clustering techniques together with a regional and local meteorological database is the scientific novelty of this work. It allows us to better understand the aerosol optical and microphysical properties and improving our understanding of the uncertainties involved in the radiative forcing via modifications in atmospheric warming or cooling by inferred aerosol types. Six different aerosol types dominated with coarse-mode (fine-) sizes of PUD, POD, and POC (BCD, OCD, and NOA) were identified based on their size distributions and absorption capabilities following the two different approaches (SSA_{440} versus

FMF_{500} and $AANG_{440\text{-}870}$ versus $EANG_{440\text{-}870}$) over the sites. However, both methods are found to be well associated with each other and revealed a similar type of aerosols.

The distinct seasonal discrepancies between both the sites highlight the dominance of PUD (POC) type of aerosols, with the highest contribution of 71.63% (28.24%) during summer in Karachi (Lahore) site, respectively. The mean SSA and ASY at Karachi and Lahore both were highest in the NOA and PUD type, respectively, considered to be more irregular size than other classes. Seasonally, high AOT_{440} (1.43±0.51) with corresponding high SSA_{440} (0.97±0.01) was noticed during autumn for NOA type at Lahore. At the same time, the lowest was found for BCD aerosol type with mean AOT_{440} (0.25±0.04) and corresponding low SSA_{440} (0.83±0.03) at Karachi site, suggesting the dominance of significant anthropogenic emissions (absorbing fine mode) aerosols, while the former is associated with scattering-type (dust particles).

The CWT analysis revealed that potential sources of Dust at Karachi and POC over Lahore were found dominating among inferred aerosol types, with a considerable influence of CWT_{Dust} >0.9 followed by CWT_{POC} (~0.8) suggesting the air masses are local as well as transported from distinct sources (from natural, and anthropogenic origin) to the study areas. The highest atmospheric forcing of +60.01 W m^{-2} (+80.07 W m^{-2}) was observed for Karachi (Lahore), with the corresponding heating rate of 2.48 $Kday^{-1}$ (2.05 $Kday^{-1}$) for BCD type. While, the lowest value of +30.51 W m^{-2} (+43.07 W m^{-2}), with the corresponding heating rate of 1.48 $Kday^{-1}$ (1.53 $Kday^{-1}$), was observed for NOA type of aerosol during the study period. However, the ARFEs at the TOP was found maximum (minimum) as -80 W m^{-2} τ^{-1}(-20 W m^{-2} τ^{-1}) for PUD (BCD) type during winter (summer), respectively, at both the sites suggesting, absorbing aerosols produce a lower ARFEs at the top of the atmosphere.

Appendix A. Supporting Material

The supplement material about the text, figures, and tables related to this article is available online at https://iopscience.iop.org/journal/1748-9326.

CREdit of the author(s) contribution statement

Rehana Khan: Formal analysis, Methodology, Visualization, Investigation, Writing-Original Draft. **Kanike Raghavendra Kumar**: Conceptualization, Resources, Supervision, Writing-review and editing. **Tianliang Zhao**: Validation, Supervision, Project Administration, Funding Acquisition, Writing-review and editing. **Gohar Ali**: Methodology, Data curation.

Conflicts of interest

The authors declare that they have no competing financial interests or personal relationships that could have appeared to influence the work reported in this article.

Funding sources

This work was supported by the National Key Research and Development Program of China (Grant No. 2016YFC0203501), and the National Natural Science Foundation of China (Grant Nos. 41805121 and 41775123). One of the authors, KRK, is grateful to the Department of Science and Technology (DST), Govt. of India, for the award of DST-FIST Level-1 (SR/FST/PS-1/2018/35) scheme to the Department of Physics, KLEF.

Acknowledgments

We owe our sincere thanks to the Principal Investigator, Prof. Brent Holben, and his staff for establishing and maintaining the AERONET station, as well as other data sources used in this study. Thanks are due for procuring the NCEP/NCAR data at http://www.esrl.noaa.gov/psd/data and meteorological variables from the Pakistan Meteorological Bureau (www.pmd.gov.pk). The authors would like to thank Prof. John Keen, the Editor-in-Chief and Prof. Freddie Taylor, Associate Editor of the journal, and the anonymous reviewers for their helpful comments and constructive suggestions towards the improvement of earlier versions of the manuscript.

Data Availability Statement

The data that support the findings of this study are available open and free to the public and can be downloaded from the homepage of AERONET at https://aeronet.gsfc.nasa.gov/.

References

Alam, K., Khan, R., Sorooshian, A., Blaschke, T., Bibi, S., & Bibi, H. (2018). Analysis of aerosol optical properties due to a Haze episode in the Himalayan foothills: Implications for climate forcing. Aerosol and Air Quality Research, 8(5).https://doi.org/10.4209/aaqr.2017.06.0222

Alam, K., Shaheen, K., Blaschke, T., Chishtie, F., Khan, H. U., & Haq, B. S. (2016). Classification of Aerosols in an Urban Environment on the Basis of Optical Measurements, Aerosol and Air Quality Research 2535–2549. https://doi.org/10.4209/aaqr.2016.06.0219

Alam, K., Trautmann, T., Blaschke, T., & Majid, H. (2012). Aerosol optical and radiative properties during summer and winter seasons over Lahore and Karachi. Atmospheric Environment, 50, 234–245. https://doi.org/10.1016/j.atmosenv.2011.12.027.

Alam, K., Trautmann, T., Blaschke, T., Subhan, F., 2014. Changes in aerosol optical properties due to dust storms in the Middle East and Southwest Asia. Remote Sens. Environ. 143, 216–227.

Bibi, H., Alam, K., & Bibi, S. (2016). In-depth discrimination of aerosol types using multiple clustering techniques over four locations in Indo-Gangetic plains. Atmospheric Research, 181, 106–114.

Bibi, S., Alam, K., Chishtie, F., Bibi, H., 2017. Characterization of absorbing aerosol types using ground and satellites based observations over an urban environment. Atmos. Environ. 150, 126–135.

Boiyo, R., Kumar, K. R., Zhao, T.L., 2019. A 10-Year Record of Aerosol Optical Properties and Radiative Forcing Over Three Environmentally Distinct AERONET Sites in Kenya , East Africa Journal of Geophysical Research : Atmospheres, 1596–1617. https://doi.org/10.1029/2018JD029461

Che, H., Qi, B., Zhao, H., Xia, X., Eck, F. Thomas., Goloub, P.,Dubovik, O., Estelles, V., Agulló, E.C., Blarel, L., Wu, Y., Zhu, J.,Du, R., Wang, Y., Wang, H., Gui, K., Yu, J., Zheng, Y.,Sun, T., Chen, Q., Shi, G., Zhang, X.2018. Aerosol optical properties and direct radiative forcing based on measurements from the China Aerosol Remote Sensing Network (CARSNET) in eastern China. Atmos. Chem. Phys., 18, 405–425, 2018.

481 Chen, H., et al. Characteristics of aerosols over Beijing and Kanpur derived from the AERONET dataset. Atmospheric Pollution Research, 2016, 7(1), 162-169

483 Choi, Y., Y. S. Ghim, and B. N. Holben (2016), Identification of columnar aerosol types under high aerosol optical depth conditions for a single AERONET site in Korea, J. Geophys. Res. Atmos., 121, 1264–1277, doi:10.1002/ 2015JD024115.

486 Dubovik, O., Sinyuk, A., Lapyonok, T., et al., 2006. Application of spheroid models to account for aerosol particle nonsphericity in remote sensing of desert dust. J. Geophys. Res. Atmos. 111, D11208. http://dx.doi.org/10.1029/2005JD006619.

489 Eck, T. F., B. N. Holben, J. S. Reid, O. Dubovik, A. Smirnov, N. T. O'Neill, I. Slutsker, and S. Kinne (1999), Wavelength dependence of the optical depth of biomass burning, urban, and desert dust aerosols, J. Geophys. Res., 104(D24), 31,333–31,349.

492 García, O.E., Díaz, A.M., Expósito, F.J., Díaz, J.P., et al., 2008. Validation of AERONET estimates of atmospheric solar fluxes and aerosol radiative forcing by ground- based broadband measurements. J. Geophys. Res. 113, D21207. doi:10.1029/ 2008JD010211.

495 Giles, D. M., B. N. Holben, T. F. Eck, A. Sinyuk, A. Smirnov, I. Slutsker, R. R. Dickerson, A. M. Thompson, and J. S. Schafer (2012), An analysis of AERONET aerosol absorption properties and classifications representative of aerosol source regions, J. Geophys. Res., 117, D17203, doi:10.1029/2012JD018127.

499 Holben, B.N., Eck, T.F., Slutsker, I.D., Tanré, D., Buis, J.P., Setzer, A., Vermote, E., Reagan, J.A., Kaufman, Y.J., Nakajima, T., Lavenu, F., Jankowiak, I. and Smirnov, A. (1998). AERONET-A Federated Instrument Network and Data Archive for Aerosol Characterization. Remote Sens. Environ. 66: 1–16.

503 Hsu, Y. K., Holsen, T. M., and Hopke, P. K.: Comparison of hy- brid receptor models to locate PCB sources in Chicago, Atmos. Environ., 37, 545–562, 2003.

505 IPCC, 2018: Summary for Policymakers. In: Global warming of 1.5°C. An IPCC Special Report on the impacts of global warming of 1.5°C above pre-industrial

507 Kang, N., Kumar, K.R., Yu, X., Yin, Y., 2016. Column-integrated aerosol optical properties and direct radiative forcing over the urban-industrial megacity Nanjing in the Yangtze River Delta, China. Environmental Science and Pollution Research, 23, 17532-17552.

510 Kaskaoutis, D.G., Singh, R.P., Gautam, R., Sharma, M., Kosmopoulos, P.G., Tripathi, S.N., 2012. Variability and trends of aerosol properties over Kanpur, northern India using AERONET data (2001–10). Environ. Res. Lett. 7, 024003.

513 Khan, R., Kumar, K. R., & Zhao, T. (2019). The climatology of aerosol optical thickness and radiative effects in Southeast Asia from 18-years of ground-based observations. Environmental Pollution, 254, 113025.

516 Kokkalis, P., Al Jsar, H., Solomas, S., Raptis, P.I., Al Hendi, H., Amiridis, V., et al., 2018. Long-term ground-based measurements of aerosol optical depth over Kuwait city. Remote Sens. 10, 1807. https://doi.org/10.3390/rs10111807.

519 Kumar KR, Sivakumar V, Reddy RR, Gopal KR, Adesina AJ (2013) Inferring wavelength dependence ofAOD and Ångström exponent over a sub-tropical station in South Africa using AERONET data: influence ofmeteorology, long-range transport and curvature effect. Sci Total Environ 461:397–408.

523 Kumar, K. R., Kang, N., Sivakumar, V., & Griffith, D. (2017). Temporal characteristics of columnar aerosol optical properties and radiativeforcing (2011-2015) measured at AERONET's Pretoria_CSIR_DPSS site in South Africa. Atmospheric Environment, 165, 274–289.

527 Kumar, K.R., Boiyo, R., Khan, R., Kang, N., Yu, X., Sivakumar, V., Griffith, D., Devi, NL., 2020. Multi-year analysis of aerosol optical properties and implications to radiative forcing over urban Pretoria, South Africa. Theoretical and Applied Climatology 1-15, doi:10.1007/s00704-020-03183-7.

531 Kumar, M., Parmar, K. S., Kumar, D. B., Mhawish, A., Broday, D. M., Mall, R. K., Banerjee, T. 2018. Long-term aerosol climatology over Indo-Gangetic Plain: Trend, prediction and potential source fields. Atmos. Environ. 180, 37-50.

534 Lee J, Kim J, Song CH, Kim SB, Chun Y, Sohn BJ, Holben BN (2010) Characteristics of aerosol types from AERONET sunphotometer measurements. Atmos Environ 44:3110–3117.

536 Moreno, I., Alados, I., Guerrero-Rascado, J. L., Lyamani, H., Pérez-Ramírez, D., Olmo, F. J., Alados-Arboledas, L. (2019). Contribution to column-integrated aerosol typing based on Sun-photometry using different criteria. Atmospheric Research, 224(March), 1–17.

539 Ricchiazzi, P., Yang, S., Gautier, C., Sowle, D., 1998. SBDART: a research and teaching software tool for plane-parallel radiative transfer in the Earth's atmosphere. Bull. Am. Meteorol. Soc. 79, 2101–2114.

542 Rupakheti, D., Kang, S., Rupakheti, M., Cong, Z., Panday, A. K., & Holben, B. N. (2019). Identification of absorbing aerosol types at a site in the northern edge of Indo-Gangetic Plain and a polluted valley in the foothills of the central Himalayas. Atmospheric Research, 223(January), 15–23. https://doi.org/10.1016/j.atmosres.2019.03.003

546 Shaheen, K., Shah, Z., Suo, H., Liu, M., Ma, L., Alam, K., Gul, A., Cui, J., Li, C., Wang, Y., Khan, S.A., Khan, S.B., Aerosol clustering in an urban environment of Beijing during (2005-2017), Atmospheric Environment (2019).

549 Shin, S.K., Tesche, M., Noh, Y., Muller, D. 2019. Aerosol type classification based on AERONET version3 inversion products. Atmos. Meas. Tech. Discuss., http://doi.org/10.5194/amt-2019-122.

552 Srivastava, A.K., Tripathi, S.N., Sagnik, D., Kanawade, V.P., Tiwari, S., 2012. Inferring aerosol types over the Indo-Gangetic Basin from ground based sunphotometer measurements. Atmos. Res. 109-110, 64–75.

555 Tiwari, S., Srivastava, A. K., Singh, A. K., & Singh, S. (2015). Identification of aerosol types overIndo-Gangetic Basin : implications to optical properties and associated radiative forcing. https://doi.org/10.1007/s11356-015-4495-6.

558 Yu XN, Lu R, Kumar KR, Ma J, Zhang Q, Jiang Y, Kang N, Yang S, Wang J, Li M (2016) Dust aerosol properties and radiative forcing observed in spring during 2001-2014 over urban Beijing, China. Environ Sci Pollut Res 23:15432–15442.

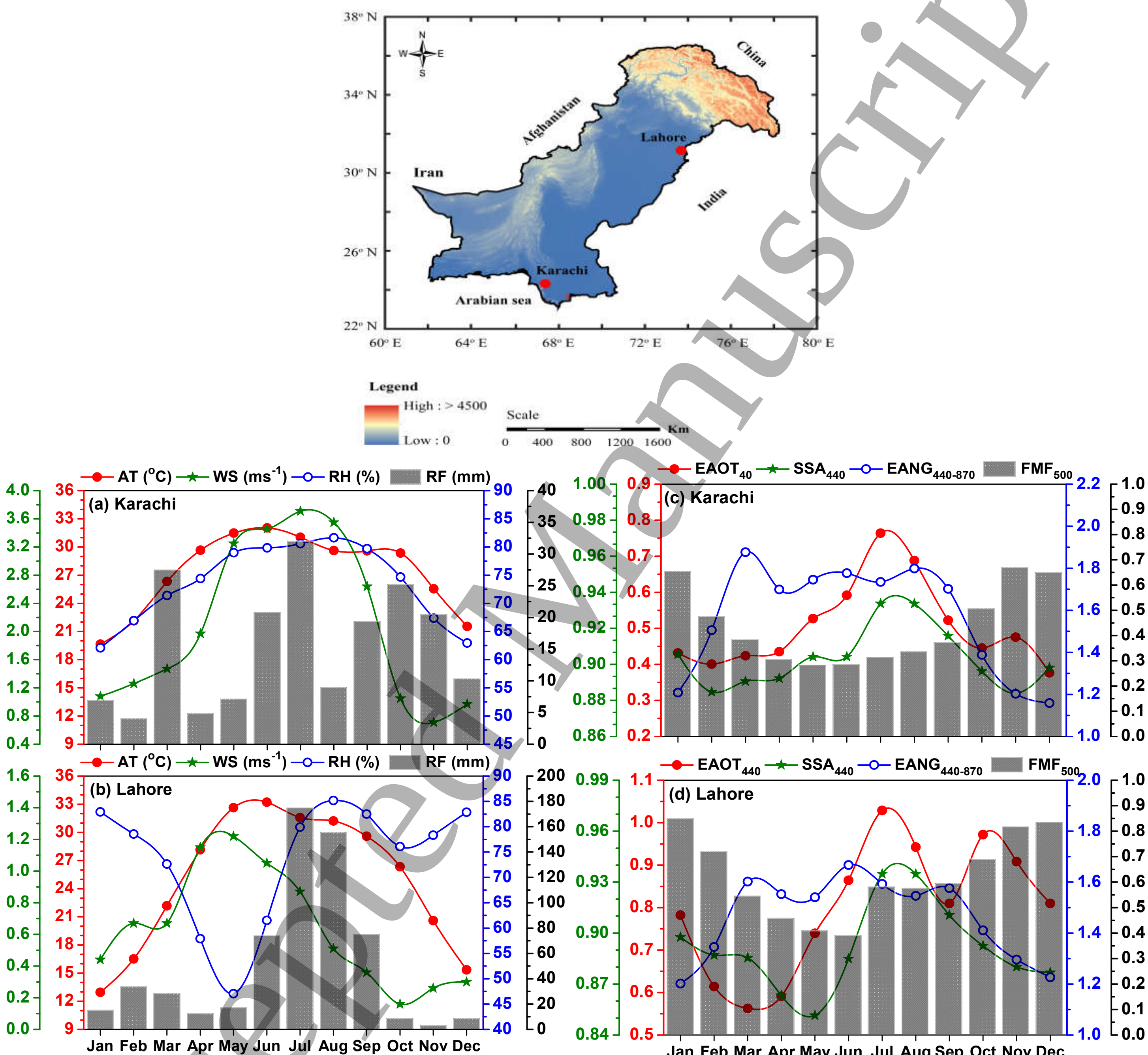

Fig. 1. Topographical map (color scale shown below in km) of the study domain where the location of two AERONET sites used in this work are identified with red color solid circles. The monthly mean variations of meteorological parameters and aerosol optical properties observed at Karachi and Lahore during the study period.

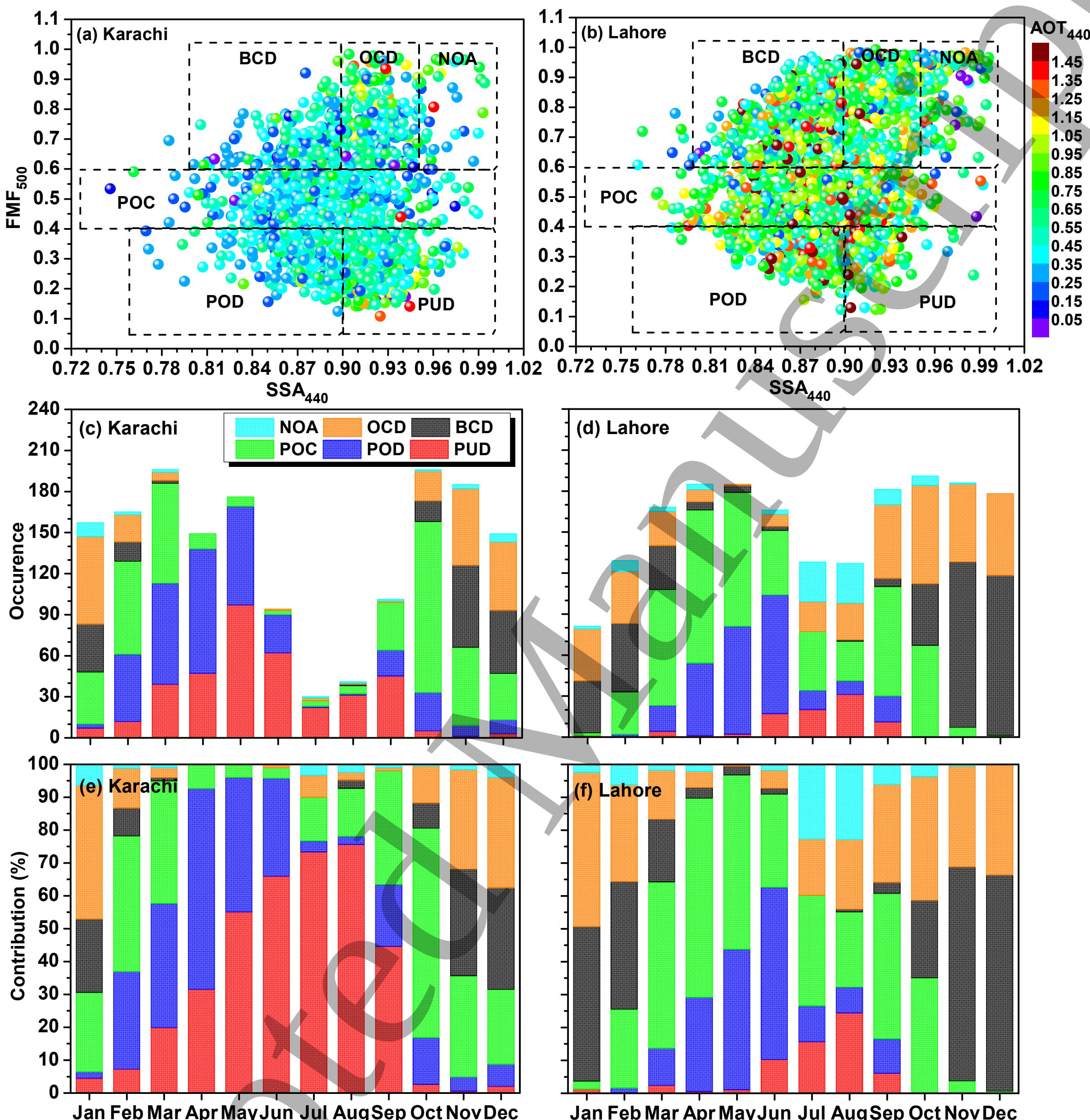

Fig. 2. (a-b) Scatter plots representing the cluster technique between FMF_{500} and SSA_{440} to discriminate scattering and absorbing aerosol types. The colored symbols correspond to the varying AOT_{440} with the threshold limits shown as dashed lines during the entire study period over (a) Karachi and (b) Lahore. Monthly variations in the observed aerosol types with their (c, d) occurrence of frequencies and (e, f) percentage contributions over Karachi and Lahore.

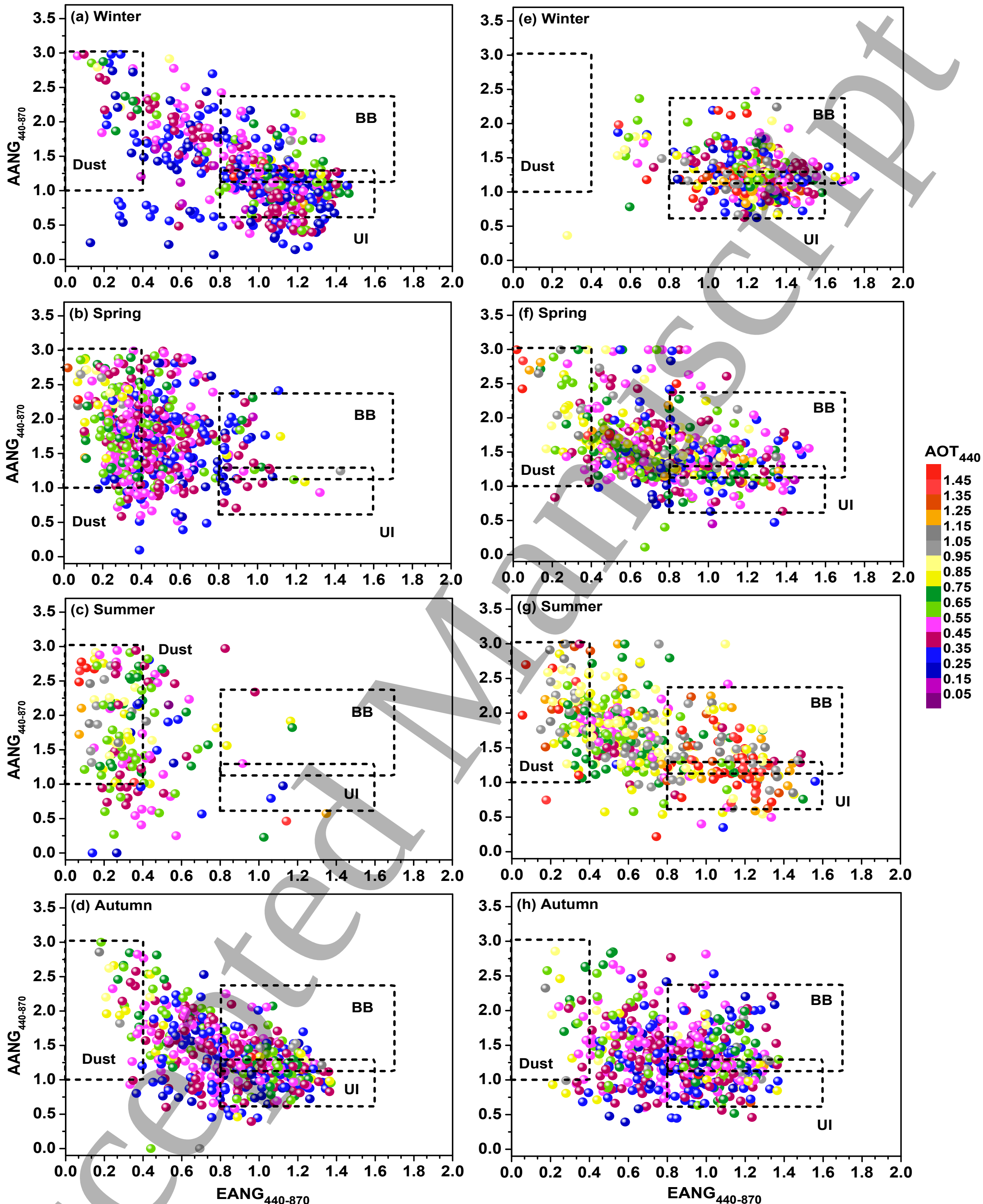

Fig. 3. Scatter plots representing the cluster technique between AANG and ANG to discriminate scattering and absorbing aerosol types on seasonal basis. The colored symbols correspond to the varying AOT_{440} with the threshold limits shown as dashed lines during the entire study period over (a-d) Karachi and (e-h) Lahore. The labels Dust, BB (biomass burning) and UI (Urban/industrial) corresponds to PUD, BCD and NOA, respectively.

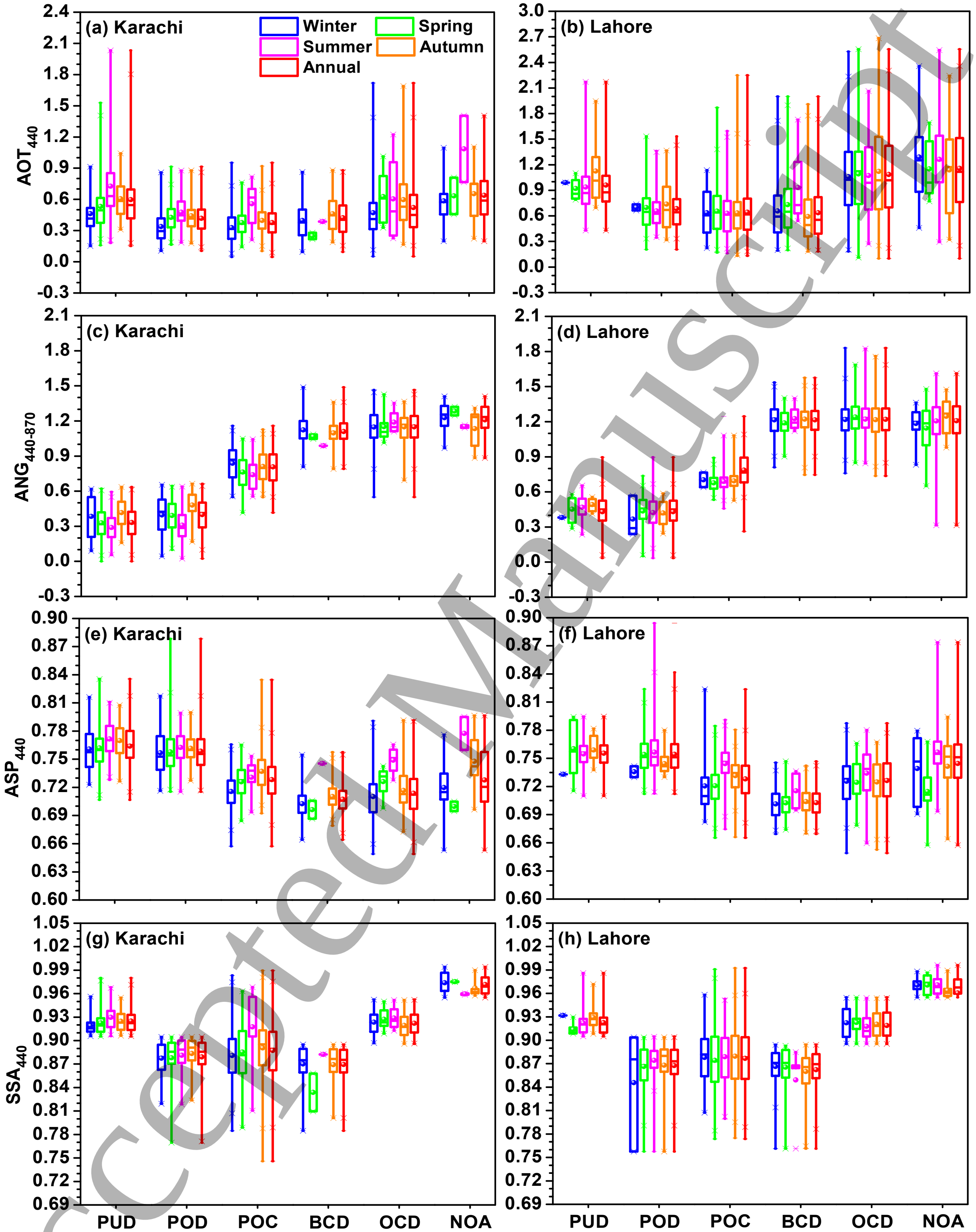

Fig. 4. Box-whisker plots of aerosol optical properties presenting the annual and seasonal changes for the inferred aerosol types observed at Karachi and Lahore.

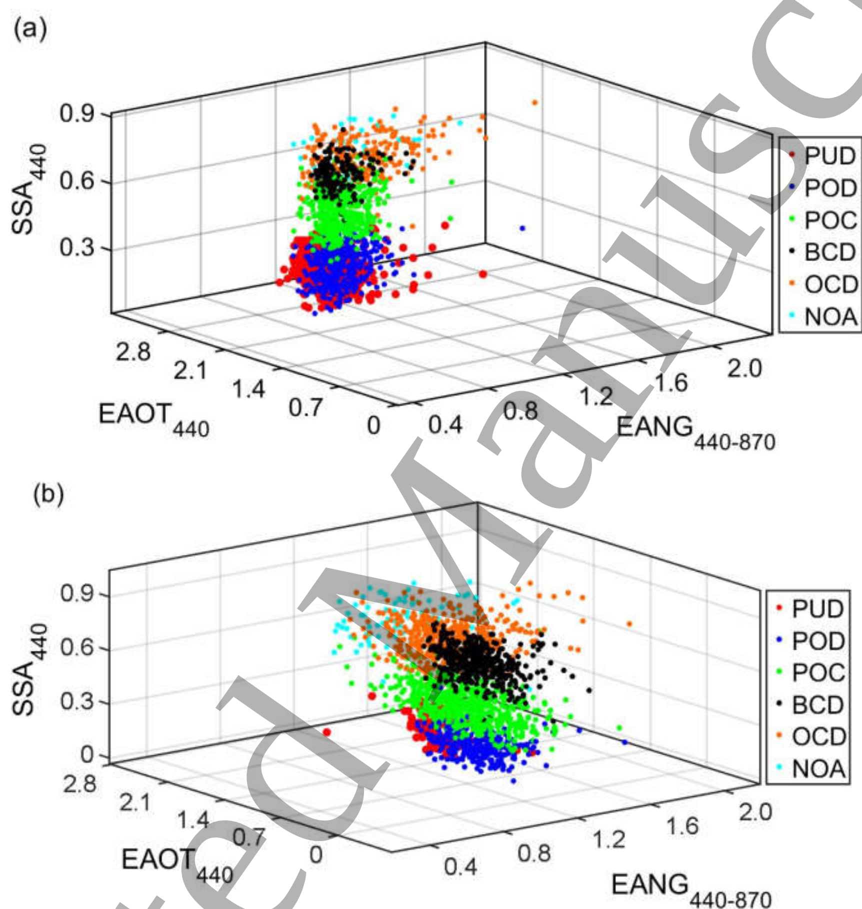

Fig. 5. 3D representation of aerosol optical properties for the inferred aerosol types at Karachi and Lahore.

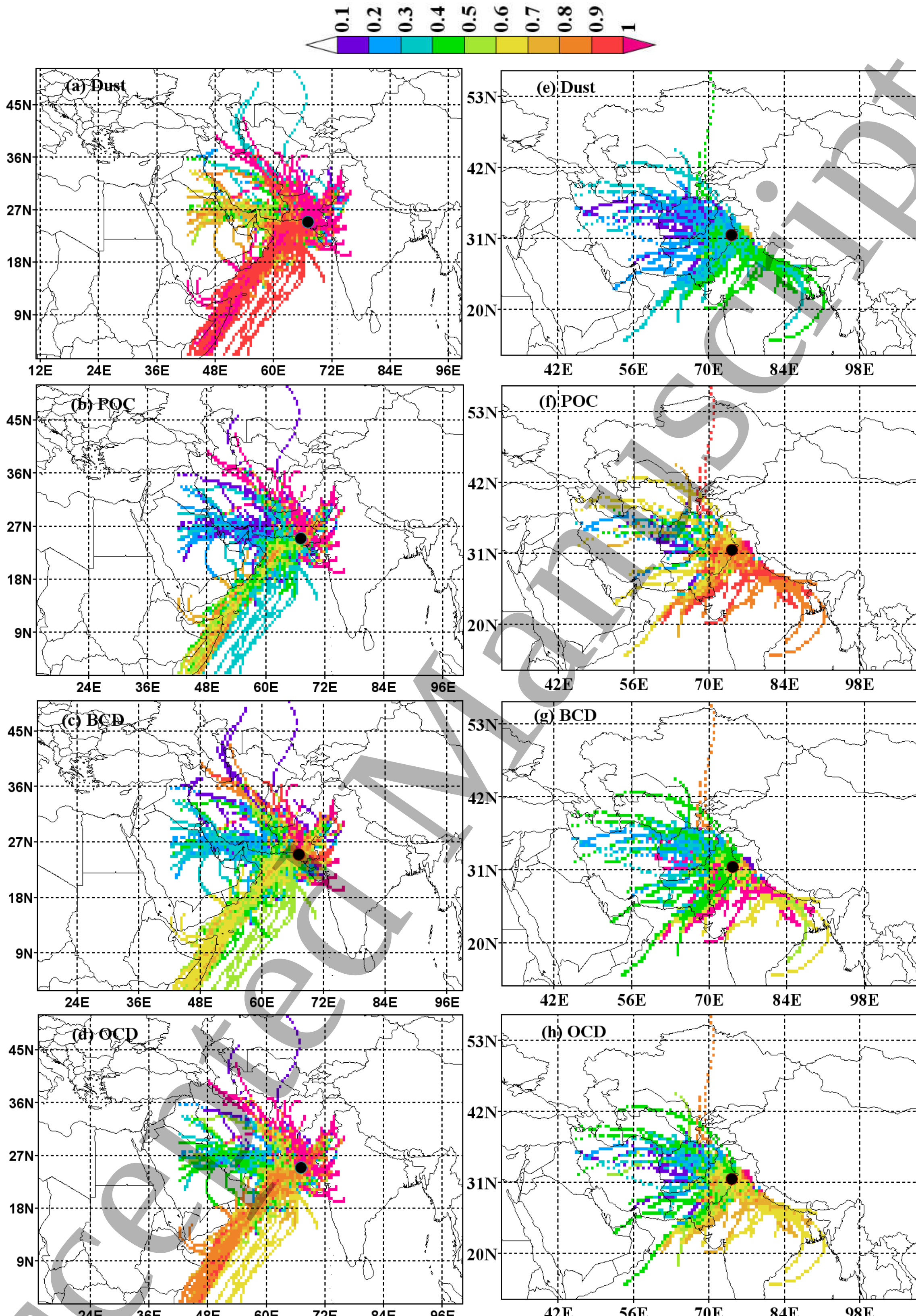

Fig. 6. The CWT analysis obtained for different aerosol types utilizing the HYSPLIT back ward trajectories observed at Karachi (a-d) and Lahore (e-h) during the entire study period. The concentrations shown along the trajectories correspond to the input quantity (here AOT_{440}), where in the corresponding colour scale is shown on the top of panels. The location of AERONET site is denoted with a black solid circle in all the panels.

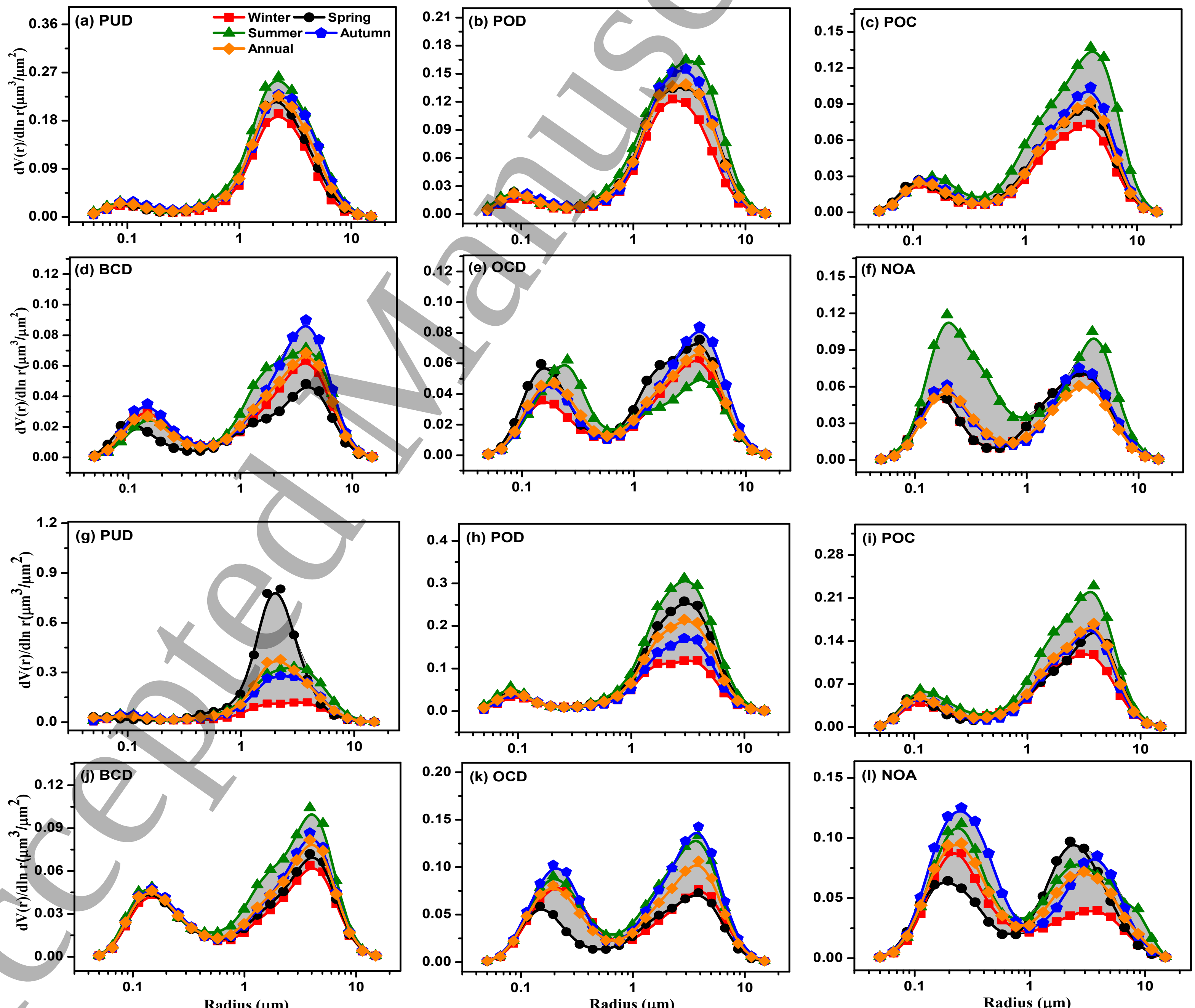

Fig. 7. Annual and seasonal changes of volume particle size distribution for the inferred aerosol types, observed at Karachi (a-f) and Lahore (g-l) during the entire study period. The shaded portion within the distribution corresponds to the mean standard deviation.

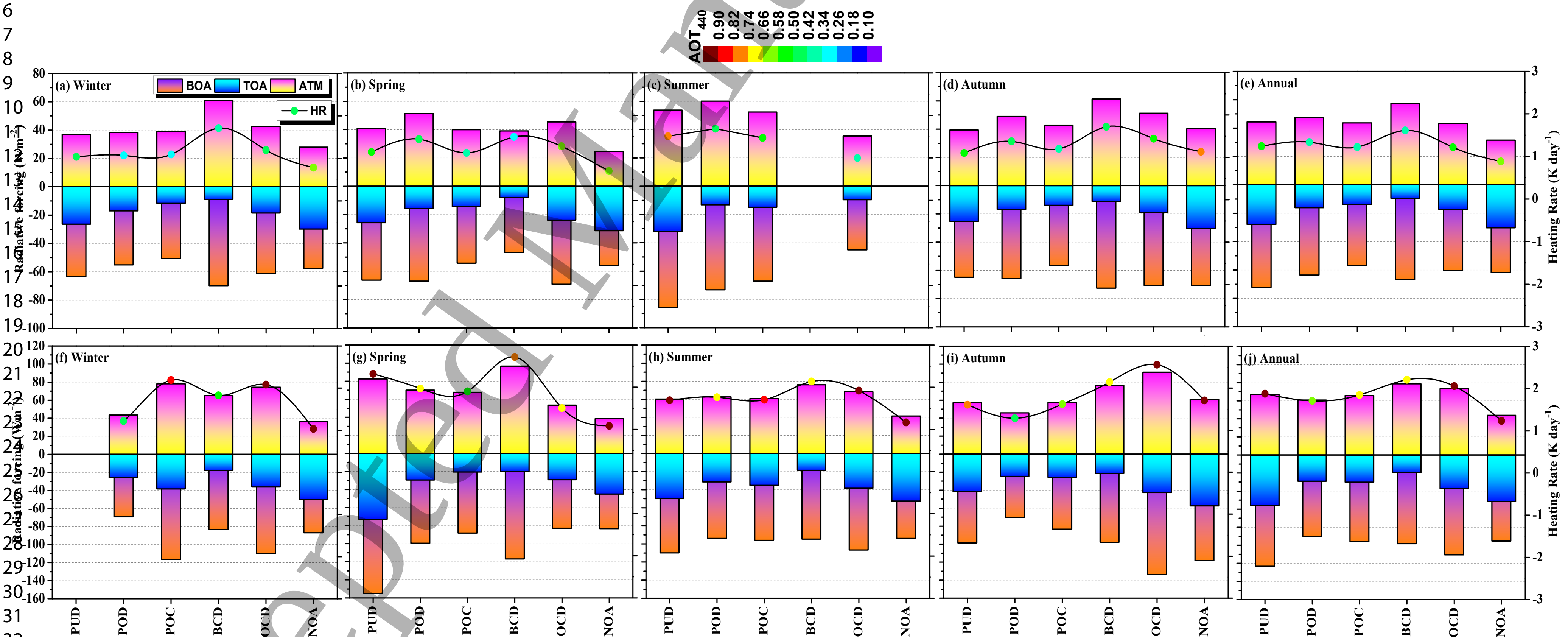

Fig. 8. Seasonal and annual changes in SBDART-modelled ARF (in W m^{-2}) and ARFE (in W m^{-2} τ^{-1}) at the BOA, TOA, and ATM for different aerosol types estimated at Karachi (a-e) and Lahore (f-j). Whereas, the atmospheric HR is shown as line+symbol (solid circle) and the colour to the symbols indicate the change in AOT_{440} with the colour scale noted on the top.

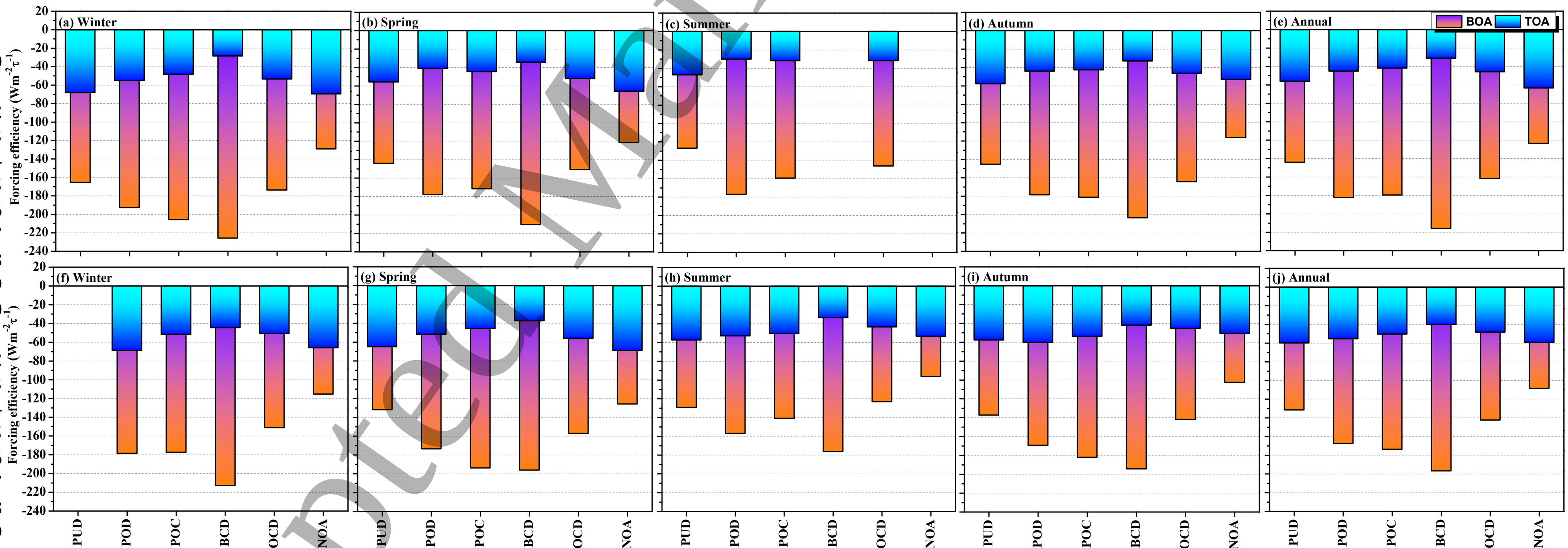

Fig. 8. (Continued).

Table 1. The annual and seasonal variations of different aerosol optical parameters and percent contribution for the inferred aerosol types observed at Karachi and Lahore sites during 2007-2018. The magnitudes of respective parameters presented are unit less.

Karachi								
Aerosol Type		AOT_{440}	$ANG_{440-870}$	SSA_{440}	ASP_{440}	$AANG_{440-870}$	FMF_{500}	%
PUD	Winter	0.46±0.21	0.38±0.17	0.92±0.01	0.76±0.02	2.19±0.57	0.31±0.08	2.34
	Spring	0.53±0.22	0.33±0.14	0.92±0.01	0.76±0.02	1.97±0.67	0.27±0.06	35.52
	Summer	0.73±0.36	0.29±0.12	0.93±0.01	0.77±0.02	1.96±0.71	0.25±0.05	71.63
	Autumn	0.61±0.17	0.42±0.12	0.92±0.01	0.77±0.02	1.92±0.58	0.31±0.05	15.88
	Annual	0.59±0.28	0.33±0.13	0.92±0.01	0.76±0.02	1.96±0.69	0.27±0.06	31.9
POD	Winter	0.34±0.16	0.40±0.15	0.88±0.02	0.76±0.02	1.76±0.71	0.30±0.07	4.31
	Spring	0.43±0.13	0.39±0.13	0.88±0.03	0.76±0.02	1.69±0.56	0.30±0.06	46.58
	Summer	0.48±0.14	0.31±0.13	0.88±0.02	0.76±0.02	1.33±0.56	0.26±0.05	11.85
	Autumn	0.44±0.14	0.48±0.11	0.88±0.02	0.76±0.02	1.73±0.55	0.34±0.04	12.47
	Annual	0.41±0.13	0.39±0.13	0.87±0.02	0.75±0.02	1.68±0.59	0.30±0.06	20.92
POC	Winter	0.33±0.14	0.84±0.14	0.88±0.03	0.72±0.02	1.37±0.49	0.51±0.06	25.94
	Spring	0.38±0.12	0.76±0.13	0.89±0.04	0.73±0.02	1.70±0.56	0.46±0.05	16.2
	Summer	0.56±0.19	0.74±0.14	0.92±0.05	0.73±0.02	1.37±0.74	0.47±0.05	10.38
	Autumn	0.40±0.12	0.81±0.13	0.89±0.04	0.74±0.02	1.35±0.44	0.50±0.06	43.08
	Annual	037±0.13	0.80±0.13	0.88±0.03	0.72±0.02	1.43±0.51	0.49±0.06	24.77
BCD	Winter	0.40±0.17	1.12±0.11	0.87±0.02	0.70±0.02	0.94±0.38	0.69±0.06	28.53
	Spring	0.25±0.04	1.07±0.03	0.83±0.03	0.70±0.01	1.46±0.43	0.63±0.02	0.34
	Summer	0.38±0.00	0.98±0.00	0.88±0.00	0.7±0.00	2.33±0.00	0.68±0.0	0.81
	Autumn	0.46±0.16	1.10±0.10	0.87±0.03	0.71±0.01	1.15±0.24	0.69±0.08	13.36
	Annual	0.42±0.16	1.11±0.10	0.86±0.02	0.70±0.01	1.04±0.36	0.69±0.07	8.77
OCD	Winter	0.47±0.25	1.15±0.14	0.92±0.01	0.71±0.02	1.13±0.36	0.74±0.09	34.86
	Spring	0.63±0.26	1.15±0.15	0.93±0.01	0.73±0.02	1.52±0.49	0.71±0.11	1.02
	Summer	0.60±0.46	1.19±0.11	0.93±0.02	0.75±0.02	1.04±0.55	0.69±0.08	3.39
	Autumn	0.60±0.29	1.15±0.12	0.92±0.02	0.72±0.02	1.15±0.34	0.78±0.12	14.16
	Annual	0.51±0.27	1.14±0.13	0.92±0.01	0.71±0.02	1.15±0.36	0.75±0.10	11.85
NOA	Winter	0.58±0.21	1.23±0.14	0.97±0.01	0.72±0.03	0.97±0.01	1.22±0.35	4.01
	Spring	0.63±0.25	1.28±0.05	0.98±0.00	0.70±0.01	0.98±0.00	1.01±0.01	0.34
	Summer	1.09±0.45	1.15±0.01	0.96±0.00	0.78±0.02	0.96±0.00	1.19±1.03	1.92
	Autumn	0.65±0.34	1.13±0.19	0.97±0.01	0.75±0.04	0.97±0.01	1.07±0.39	1.04
	Annual	0.64±0.27	1.21±0.14	0.97±0.01	0.72±0.03	0.97±0.01	1.18±0.39	1.79

Table 1. (Continued).

		Lahore						
Aerosol Type		AOT_{440}	$ANG_{440-870}$	SSA_{440}	ASP_{440}	$AANG_{440-870}$	FMF_{500}	%
PUD	Winter	0.86±0.00	0.52±0.00	0.91±0.00	0.73±0.00	1.53±0.00	0.39±0.00	0.41
	Spring	1.30±0.61	0.15±0.14	0.93±0.03	0.76±0.03	2.68±0.91	0.19±0.06	1.33
	Summer	0.95±0.27	0.38±0.12	0.92±0.02	0.75±0.01	2.07±0.55	0.30±0.05	16.76
	Autumn	0.81±0.11	0.43±0.09	0.92±0.01	0.76±0.01	2.16±0.51	0.33±0.04	2.03
	Annual	0.96±0.31	0.37±0.14	0.92±0.02	0.76±0.02	2.12±0.59	0.30±0.06	5.13
POD	Winter	0.45±0.16	0.55±0.02	0.89±0.01	0.74±0.01	1.70±0.24	0.38±0.01	0.52
	Spring	0.68±0.27	0.43±0.13	0.87±0.02	0.75±0.02	1.77±0.46	0.32±0.05	27.55
	Summer	0.74±0.32	0.40±0.13	0.88±0.02	0.76±0.02	1.77±0.37	0.31±0.05	23.74
	Autumn	0.51±0.10	0.54±0.12	0.89±0.01	0.74±0.01	1.88±0.38	0.35±0.03	3.5
	Annual	0.68±0.27	0.43±0.13	0.87±0.02	0.75±0.02	1.77±0.46	0.32±0.05	13.83
POC	Winter	0.56±0.34	0.81±0.21	0.87±0.04	0.72±0.03	1.51±0.38	0.51±0.07	9.02
	Spring	0.58±0.27	0.79±0.13	0.86±0.03	0.72±0.02	1.49±0.45	0.48±0.06	54.7
	Summer	0.85±0.25	0.73±0.12	0.91±0.03	0.74±0.02	1.57±0.51	0.47±0.06	28.24
	Autumn	0.62±0.21	0.82±0.13	0.89±0.03	0.73±0.02	1.64±0.41	0.50±0.06	27.68
	Annual	0.64±0.28	0.79±0.14	0.88±0.04	0.73±0.02	1.54±0.45	0.49±0.06	29.91
BCD	Winter	0.57±0.30	1.25±0.13	0.86±0.02	0.70±0.02	1.24±0.27	0.79±0.08	50.47
	Spring	0.61±0.31	1.18±0.15	0.87±0.02	0.70±0.02	1.34±0.27	0.68±0.06	8.33
	Summer	0.64±0.27	1.11±0.15	0.88±0.01	0.72±0.02	1.05±0.29	0.67±0.10	0.87
	Autumn	0.72±0.36	1.18±0.12	0.87±0.02	0.70±0.01	1.28±0.25	0.76±0.09	30.64
	Annual	0.63±0.33	1.21±0.13	0.86±0.13	0.70±0.01	1.26±0.26	0.77±0.09	22.58
OCD	Winter	1.02±0.52	1.25±0.18	0.92±0.02	0.72±0.02	1.22±0.29	0.88±0.08	36.69
	Spring	0.63±0.39	1.25±0.18	0.92±0.02	0.71±0.03	1.39±0.44	0.72±0.08	6.76
	Summer	1.09±0.41	1.15±0.17	0.94±0.02	0.75±0.01	1.27±0.44	0.78±0.11	14.62
	Autumn	1.27±0.63	1.22±0.12	0.92±0.02	0.73±0.02	1.32±0.31	0.84±0.11	32.73
	Annual	1.11±0.58	1.22±0.16	0.92±0.02	0.73±0.02	1.29±0.34	0.84±0.11	22.7
NOA	Winter	0.99±0.51	1.30±0.20	0.97±0.01	0.73±0.02	0.97±0.01	1.29±0.40	2.89
	Spring	0.87±0.47	1.24±0.20	0.97±0.01	0.71±0.05	0.97±0.01	1.35±0.54	1.32
	Summer	1.28±0.51	1.18±0.19	0.97±0.01	0.75±0.03	0.97±0.01	1.24±0.05	15.77
	Autumn	1.43±0.68	1.25±0.17	0.97±0.01	0.75±0.03	0.97±0.01	1.34±0.64	3.43
	Annual	1.25±0.56	1.20±0.19	0.97±0.01	0.74±0.03	0.97±0.01	1.20±0.19	5.85

Table 2. Annual means of AERONET retrieved volume concentration (V_F, V_C, V_T), volume median radius (VMR_F, VMR_C, VMR_T), Standard deviation (σ_F, σ_C, σ_T) and effective radius ($Reff_F$, $Reff_C$, $Reff_T$) in different particle modes (fine, coarse, total) for inferred aerosol types during 2001-2018. The units of V, VMR and R_{eff} are $\mu m^3 \mu m^{-2}$ and μm, respectively, while σ is unit less.

Aerosol Type	V_F	$Reff_F$	VMR_F	V_C	$Reff_C$	VMR_C	V_T	$Reff_T$	VMR_T
	Karachi								
PUD	0.37±0.01	0.12v0.01	0.14±0.02	0.37±0.21	1.91±0.17	2.33±0.25	0.41±0.22	0.79±0.17	1.77±0.23
POD	0.02±0.01	0.11±0.01	0.13±0.02	0.24±0.10	1.98±0.28	2.44±0.33	0.27±0.11	0.76±0.16	1.80±0.28
POC	0.03±0.01	0.13±0.01	0.14±0.01	0.15±0.06	2.14±0.21	2.68±0.28	0.18±0.07	0.63±0.11	1.66±0.26
BCD	0.03±0.01	0.14±0.01	0.16±0.01	0.11±0.05	2.34±0.17	2.94±0.19	0.15±0.06	0.50±0.08	1.42±0.25
OCD	0.05±0.03	0.16±0.02	0.17±0.02	0.11±0.05	2.32±0.31	2.86±0.31	0.16±0.08	0.46±0.09	1.23±0.30
NOA	0.07±0.04	0.18±0.03	0.20±0.03	0.09±0.04	2.36±0.40	2.82±0.43	0.17±0.07	0.40±0.08	0.95±0.25
	Lahore								
PUD	0.06±0.02	0.12±0.02	0.14±0.02	0.59±0.29	1.96±0.22	2.38±0.33	0.65±0.30	0.76±0.19	1.76±0.32
POD	0.05±0.02	0.10±0.01	0.12±0.02	0.44±0.23	2.11±0.22	2.58±0.28	0.49±0.24	0.70±0.15	1.84±0.29
POC	0.06±0.03	0.13±0.02	0.14±0.02	0.27±0.13	2.14±0.24	2.69±0.30	0.33±0.15	0.57±0.12	1.58±0.30
BCD	0.06±0.03	0.15±0.02	0.17±0.02	0.13±0.08	2.41±0.23	3.01±0.25	0.19±0.10	0.42±0.08	1.18±0.27
OCD	0.12±0.07	0.18±0.03	0.20±0.04	0.17±0.09	2.45±0.32	2.98±0.33	0.29±0.14	0.41±0.08	1.01±0.28
NOA	0.15±0.07	0.20±0.04	0.23±0.04	0.18±0.45	2.42±0.47	2.89±0.56	0.33±0.46	0.39±0.24	0.82±0.54